DOI: 10.1002/ejic.201000112

Cyano-Bridged 2D Bimetallic 4f–3d Arrays with Monolayered Stair-Like, Brick-Wall-Like, or Bilayered Topologies – Rational Syntheses and Crystal Structures

Wen-Tong Chen,[a,b] A-Qing Wu,[a] Guo-Cong Guo,*[a] Ming-Sheng Wang,[a] Li-Zhen Cai,[a] and Jin-Shun Huang[a]

Keywords: Lanthanides / N ligands / Synthesis design / Self-assembly / Prussian blue complexes

Three series of fourteen cyano-bridged 2D Ln^{III}–Fe^{III} or Ln^{III}–Co^{III} complexes, $[Ln(dmso)_2(H_2O)(\mu\text{-}CN)_4Fe(CN)_2]_n$ [Ln = Gd (**1**) and Er (**2**)], $[Ln(dmso)_2(H_2O)_3(\mu\text{-}CN)_3M(CN)_3]_n$ [La–Fe (**3**) and Pr–Co (**4**)], $[Ln(dmf)_2(H_2O)_3(\mu\text{-}CN)_3M(CN)_3]_n{\cdot}nH_2O$ [Nd–Fe (**5**), Gd–Fe (**6**), Dy–Fe (**7**), Er–Fe (**8**), Nd–Co (**9**), and Gd–Co (**10**)], $[Ln(dmso)_2(H_2O)_3(\mu\text{-}CN)_3Co(CN)_3]_n{\cdot}nH_2O$ [Ln = Pr (**11**), Nd (**12**), and Sm (**13**)], and $[Er(dmf)(H_2O)_3(\mu\text{-}CN)_4Co(CN)_2]_n{\cdot}nH_2O$ (**14**) (dmso = dimethyl sulfoxide; dmf = *N*,*N*′-dimethylformamide) were rationally prepared by the ball-milling method, and their structures were characterized. The crystal structures of **1** and **2** reveal a sevenfold coordination environment of the Ln^{3+} ions and a 2D stair-like structure, while those of **3**–**13** show an eightfold coordination environment of the Ln^{3+} ions and a 2D monolayered brick-wall-like topology and that of **14** exhibits an eightfold coordination environment of the Er^{3+} ions and a 2D bilayered topology. The relationship between the crystal structures and the controllable synthesis was also discussed.

Introduction

In recent years, considerable research efforts have been focused on the design and elaboration of molecule-based magnetic materials of cyano-bridged bimetallic assemblies because of their remarkable magnetic, magnetic-optical, optoelectronic properties, and so forth.[1] A series of 3D cyano-bridged bimetallic assemblies of prussian blue analogues, resulting from the reactions of $[M(CN)_6]^{n-}$ (M = transition metal atom) and simple metal ions, have been synthesized and studied structurally and magnetically since 1976.[2] However, the difficulty in obtaining single crystals suitable for X-ray diffraction analysis impedes the investigations on the 3D assemblies. Furthermore, the face-centered cubic structures (based on powder XRD results) of the 3D assemblies usually exhibit low or nonexistent magnetic anisotropy.[2] To overcome these problems, one strategy is to incorporate organic ligands into the 3D assemblies to increase their solubility and yield hybrid prussian blue complexes. Nowadays, many hybrid prussian blue assemblies (4f–3d and 3d–3d) with low dimensionalities have been obtained by reacting $[M(CN)_6]^{n-}$ anions with metal–organic complex cations.[3,4] It is noteworthy that 4f–3d hybrid prussian blue assemblies are relatively rare and poorly investigated,[3] in comparison with numerous 3d–3d hybrid prussian blue assemblies that have been well studied structurally and magnetically.[4] To the best of our knowledge, 4f–3d hybrid prussian blue assemblies are often synthesized by conventional solution methods, mostly yielding discrete 4f–3d complexes, the coordination environment of Ln^{3+} ions being easily saturated by solvent molecules,[5] which impede more CN^- groups from the $[M(CN)_6]^{n-}$ species to bridge Ln^{3+} ions to yield 1-, 2- or 3D structures. In order to obtain higher-dimensional 4f–3d hybrid prussian blue complexes, the amount of solvent used should be reduced as much as possible in the reactive system. Our strategy was to employ the ball-milling method to effectively control the molar ratio of reactants and solvents. As a result, we easily synthesized a series of cyano-bridged 2D 4f–3d hybrid prussian blue complexes.[6] Herein we report the design, syntheses, and structures of fourteen cyano-bridged 2D bimetallic 4f–3d hexacyanometalates with monolayered stair-like, brick-wall-like, or bilayered topologies: $[Ln(dmso)_2(H_2O)(\mu\text{-}CN)_4Fe(CN)_2]_n$ [Ln = Gd (**1**) and Er (**2**)], $[Ln(dmso)_2(H_2O)_3(\mu\text{-}CN)_3M(CN)_3]_n$ [La–Fe (**3**) and Pr–Co (**4**)], $[Ln(dmf)_2(H_2O)_3(\mu\text{-}CN)_3M(CN)_3]_n{\cdot}nH_2O$ [Nd–Fe (**5**), Gd–Fe (**6**), Dy–Fe (**7**), Er–Fe (**8**), Nd–Co (**9**), and Gd–Co (**10**)], $[Ln(dmso)_2(H_2O)_3(\mu\text{-}CN)_3Co(CN)_3]_n{\cdot}nH_2O$ [Ln = Pr (**11**), Nd (**12**), and Sm (**13**)], and $[Er(dmf)(H_2O)_3(\mu\text{-}CN)_4Co(CN)_2]_n{\cdot}nH_2O$ (**14**) (dmso = dimethyl sulfoxide; dmf = *N*,*N*′-dimethylformamide), which were prepared by a facile ball-milling method.

[a] State Key Laboratory of Structural Chemistry, Fujian Institute of Research on the Structure of Matter, Chinese Academy of Sciences,
Fuzhou, 350002, Fujian, P. R. China
Fax: 86-591-83714946
E-mail: gcguo@fjirsm.ac.cn
[b] School of Chemistry and Chemical Engineering, Jiangxi Province Key Laboratory of Coordination Chemistry, Jinggangshan University,
Ji'an, 343009, Jiangxi, P. R. China
Supporting information for this article is available on the WWW under http://dx.doi.org/10.1002/ejic.201000112.

Results and Discussion

Syntheses

Increasing the dimensionality of a structure may enhance and improve its bulk magnetic properties. Hence, the syntheses of higher-dimensional 4f–3d hybrid prussian blue complexes have attracted great attention. However, the difficulty in obtaining single crystals suitable for X-ray diffraction analysis impedes the investigation of the higher-dimensional assemblies. Incorporating organic ligands into hybrid prussian blue complexes increases their solubility and affords the corresponding single crystals for structural analyses. Traditionally, hybrid prussian blue complexes have often been synthesized by a solution reaction method, mostly yielding discrete or lower-dimensional 4f–3d complexes, the coordination environment of the lanthanide ions being easily saturated by solvent molecules, which prevents more CN^- groups from the $[M(CN)_6]^{n-}$ block from bridging the Ln^{3+} ions to form 1-, 2-, or 3D structures. To obtain higher-dimensional 4f–3d hybrid prussian blue complexes, the amount of solvent used in the reactive system should be reduced as much as possible. Our strategy was to employ the ball-milling reaction method to effectively control the molar ratio of reactants, organic ligands, and solvents. When large amounts (1 mmol) of solvent (dmf or dmso) are added to the mixtures of Ln^{3+} and $[M(CN)_6]^{n-}$, discrete complexes are obtained. By reducing the amount of solvent to 2 mL, we synthesized a 1D chain structure.[7] Upon continuing to reduce the amount of solvent to 0.5 mL, two series of complexes with 2D monolayered structures were obtained. After carefully analyzing the structural characteristics of the complexes with brick-wall-like motif, we found that these complexes have two Ln-coordinated dmf molecules spreading out from both sides of the monolayer. It is possible to substitute the dmf molecules by CN^- groups from $[M(CN)_6]^{3-}$ units by reducing the amount of dmf, yielding new 4f–3d hybrid prussian blue complexes with more complex structures. We reduced the amount of solvent (dmf or dmso) further to 0.25 mL in order to obtain higher-dimensional structures. However, we failed to synthesize the expected 3D structure. Instead, a 2D bilayered structure having one dmf substituted by CN^- was obtained. Until now, the syntheses of 3D hybrid prussian blue complexes are still a great challenge.

IR Spectra

The IR spectra of the title complexes show some sharp bands in the range 2100–2200 cm^{-1}, which are attributed to the C≡N stretching modes. The splitting of ν(C≡N) suggests the presence of both bridged and nonbridged C≡N^- ligands. The strong bands at 900–1100 cm^{-1} are assigned to the S=O (dmso) stretching vibrations for **1**–**4** and **11**–**13**, while the strong bands at 1600–1700 are assigned to the C=O (dmf) stretching vibrations for **5**–**10** and **14**.

Crystal Structures

The summary of crystallographic data and structure analyses for **1**–**14** are listed in Tables 2–5. Selected bond lengths and bond angles are given in Tables 6–10.

$[Ln(dmso)_2(H_2O)(\mu\text{-}CN)_4Fe(CN)_2]_n$ [Ln = Gd (1) and Er (2)]

X-ray diffraction analyses reveal that complexes **1** and **2** are isomorphous, and herein complex **1** is discussed in detail. An ORTEP drawing of **1** is shown in Figure 1. The structure of **1** consists of neutral 2D stair-like layers. The Gd^{3+} ion is seven-coordinate and it is bound by two O atoms from two dmso molecules [average $Gd–O_{dmso}$ 2.324(3) Å], one O atom from one water molecule [$Gd–O_{H_2O}$ 2.336(5) Å], and four N atoms from four bridging CN^- groups [average Gd–N 2.488(4) Å], yielding a distorted pentagonal bipyramid with a pentagon defined by O1W, O11, N3#2 (1/2 + *x*, 1 – *y*, 1/2 + *z*), N3#3 (1 – *x*, 1 – *y*, 1 – *z*), and O11#1 (3/2 – *x*, *y*, 3/2 – *z*) atoms, and two axial positions filled by atoms N1 and N1#1 (3/2 – *x*, *y*, 3/2 – *z*). The Fe^{3+} ion is coordinated by six cyanide groups to form a nearly regular octahedron with Fe–C and C≡N bond lengths in the ranges 1.949(4)–1.969(4) and 1.126(6)–1.140(5) Å, respectively, which are in good agreement with those reported.[8] The bridging cyanide groups coordinate to the Gd^{3+} ions in nearly linear fashion [C(3)–N(3)–Gd(1) 169.0(3)° and C(1)–N(1)–Gd(1)#1 (–*x* + 1, –*y* + 1, –*z* + 1) 170.8(3)°]. The cyano-bridged Gd···Fe distances are in the range 5.524(1)–5.600(1) Å, which is comparable with those reported.[9] Each $[Fe(CN)_6]^{3-}$ unit connects to three $[Gd(dmso)_2(H_2O)]^{3+}$ units through three nearly coplanar CN^- groups and vice versa, forming a nearly rectangular "grid" of Gd_2Fe_2 with four sides in the range 5.524(2)–5.600(1) Å. The "grids" connect to each other through vertical CN^- groups, forming a "stair" running along the *a* direction (Figure 2). The shortest intralayer Gd···Fe distance is 7.697(2) Å. Between the adjacent layers, the terminal cyanide groups interact with the coordinating O1W water molecules through O–H···N hydrogen bonds to form a 3D supramolecular hydrogen-bonding network (Figure S1).

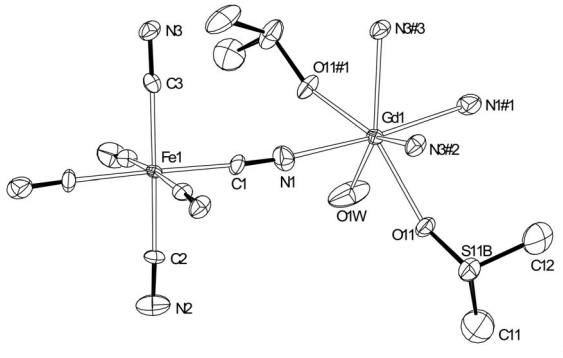

Figure 1. ORTEP drawing of **1** with 40% thermal ellipsoids; the disordered S11A atom and hydrogen atoms omitted for clarity (symmetry codes: #1: 3/2 – *x*, *y*, 3/2 – *z*; #2: 1/2 + *x*, 1 – *y*, 1/2 + *z*; #3: 1 – *x*, 1 – *y*, 1 – *z*).

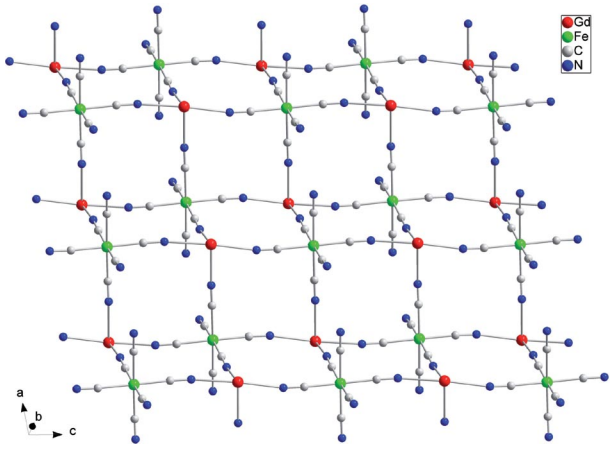

Figure 2. 2D Stair-like layer of **1**; dmso and water molecules omitted for clarity.

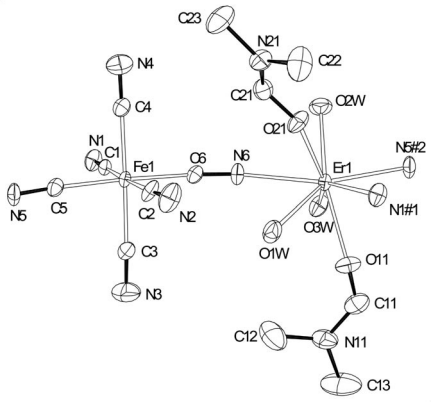

Figure 3. ORTEP drawing of **8** with 40% thermal ellipsoids; lattice water molecules and hydrogen atoms omitted for clarity (symmetry codes: #1: x, $-1+y$, z; #2: $-1+x$, $-1+y$, z).

As for $[Ln(dmso)_2(H_2O)_3(\mu\text{-}CN)_3M(CN)_3]_n$ [La–Fe (**3**) and Pr–Co (**4**)], $[Ln(dmf)_2(H_2O)_3(\mu\text{-}CN)_3M(CN)_3]_n{\cdot}nH_2O$ [Nd–Fe (**5**), Gd–Fe (**6**), Dy–Fe (**7**), Er–Fe (**8**), Nd–Co (**9**), and Gd–Co (**10**)], and $[Ln(dmso)_2(H_2O)_3(\mu\text{-}CN)_3Co(CN)_3]_n{\cdot}nH_2O$ [Ln = Pr (**11**), Nd (**12**), and Sm (**13**)], X-ray diffraction analyses reveal that complexes **3**–**13** display eightfold coordination environments of the Ln^{3+} ions and a 2D monolayered brick-wall-like topology. Herein, only the structure of **8** is discussed in detail as an example.

An ORTEP drawing of **8** is shown in Figure 3. The structure of **8** consists of neutral single layers and lattice water molecules. The Er^{3+} ion is eight-coordinate and is bound by two O atoms from two dmf molecules [average $Er–O_{dmf}$ 2.280(2) Å], three O atoms from three water molecules [average $Er–O_{H_2O}$ 2.381(2) Å], and three N atoms from three bridging CN^- groups [average Er–N 2.435(2) Å], yielding a distorted square antiprism whose top and bottom planes are defined by N6, O3W, O11, O1W and O21, N1#1(x, $-1+y$, z), N5#2($-1+x$, $-1+y$, z), O2W atoms, respectively. The Fe^{3+} ion is coordinated by six cyanide groups to yield a nearly regular octahedron with the Fe–C and C≡N bond lengths in the normal ranges of 1.937(2)–1.950(3) and 1.138(4)–1.149(3) Å, respectively. The cyano-bridged Er···Fe distances are in the range 5.309(2)–5.510(2) Å, which is comparable with those reported.[10] The $[Fe(CN)_6]^{3-}$ unit connects to three $[Er(dmf)_2(H_2O)_3]^{3+}$ units and vice versa, forming a "brick" of Er_3Fe_3, the bridging cyanides and the bridged metal ions being coplanar. The "brick" extends to generate a flat brick-wall-like layer along the a and b directions (Figure 4). The shortest intralayer Er···Fe distance is 7.626(3) Å. The flat layers are aligned parallel with separations of approximately 7.6(2) and 9.1(1) Å. The uncoordinated O4W water molecules are positioned between the distantly separated layers and linked to one terminal CN^- ligand of $[Fe(CN)_6]^{3-}$ and to the coordinated O1W and O3W water molecules by hydrogen bonds. Between the closer layers, one terminal CN^- ligand of $[Fe(CN)_6]^{3-}$ interacts with the coordinated O2W water molecules through O–H···N hydrogen bonds to connect the two layers (Figure S2).

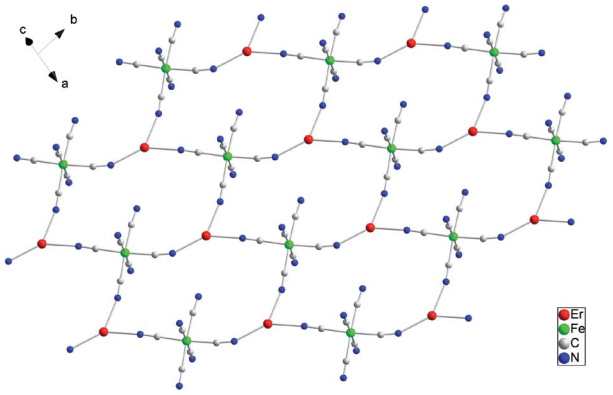

Figure 4. 2D monolayered brick-wall-like topology of **8**; dmf and water molecules omitted for clarity.

In **1**–**2**, there are four CN^- groups from one $[M(CN)_6]^{3-}$ moiety connecting to the lanthanide center to yield a 2D stair-like topology, while in **3**–**13** there are only three CN^- groups from one $[M(CN)_6]^{3-}$ moiety connecting to the lanthanide center to yield a 2D brick-wall-like structure. It is noteworthy that the 2D stair-like topologies of **1**–**2** and the 2D brick-wall-like motifs of **3**–**13** were obtained from the same synthetic procedure with the same molar ratio of reactants, but with different reactants. In our laboratory, many cyano-bridged bimetallic 4f–3d hexacyanometalates with 2D brick-wall-like structure have been successfully prepared by using dmso or dmf as solvent.[6a] We found, however, the complexes with 2D stair-like topology (**1**, **2** and those complexes we reported in the refs.[11,6b]) can only be synthesized by using dmso as solvent but not dmf, although we tried our best to use dmf as solvent to prepare such a structural topology. This may be ascribed to the fact that the steric hindrance of dmf is larger than that of dmso, preventing the fourth CN^- group from the $[M(CN)_6]^{3-}$ moiety to bridge to the lanthanide center. Therefore, the difference of the architectures of the 2D stair-like topology and the 2D brick-wall-like motif should result from the different dmso and dmf ligands, and it seems that this difference has nothing to do with the lanthanide ions, because several lan-

thanide ions occurs in both architectures. Complexes **4** and **11** are isomeric, except for lattice water molecules with space groups *Pnma* and $P2_1/c$, respectively. Complex **11** contains one lattice water molecule, which forms hydrogen-bonding interactions with coordinated water molecules and the N atom of dmso, whereas there are no lattice water and hydrogen-bonding interactions in **4**. The force of hydrogen bonds reduces the symmetry from the orthorhombic system of **4** to the monoclinic system of **11**.

[Er(dmf)(H$_2$O)$_3$(μ-CN)$_4$Co(CN)$_2$]$_n$·nH$_2$O (14)

An ORTEP drawing of **14** is shown in Figure 5. The structure of **14** consists of neutral bilayers and lattice water molecules. The Er^{3+} ion is eight-coordinate and is bound by one O atom from one dmf molecule [Er–O_{dmf} 2.251(3) Å], three O atoms from three water molecules [average Er–O_{H_2O} 2.371(4) Å], and four N atoms from four bridging CN^- groups [average Er–N 2.446(5) Å], yielding a distorted square antiprism whose top and bottom planes are defined by N1#1(*–x*, 2 – *y*, *–z*), O2W, N6, O3W and N4#2(*x*, *–*1 + *y*, *z*), N5#3(1 + *x*, *–*1 + *y*, *z*), O1W, O11 atoms, respectively. The Co^{3+} ion is octahedrally coordinated by six cyanide groups with the Co–C and C≡N bond lengths in the normal ranges of 1.870(5)–1.913(6) and 1.129(7)–1.168(6) Å, respectively. The cyano-bridged Co···Er distances are in the range 5.2814(9)–5.4506(9) Å. The $[Co(CN)_6]^{3-}$ unit uses three cyanide groups in the meridional arrangement to connect to three $[Er(dmf)(H_2O)_3]^{3+}$ units and vice versa, the bridging cyanides and the bridged metal ions being coplanar. This local molecular disposition extends to generate a flat brick-wall-like sublayer along the *a* and *b* directions (Figure 6), which is further linked by the fourth cyanide group nearly perpendicular to the layer, to form a bilayer (Figure 7). Interestingly, the structures of **8** and **14** are obviously different, although the molecular formulas of the two complexes are only slightly different. In comparison with **14**, the second dmf ligand in **8** prevents the monolayer from further linking together to form a bilayer (Figure 8). Unlike **8** and other known 2D prussian blue analogs and hybrid prussian blue complexes, which feature square-, honeycomb-, brick-

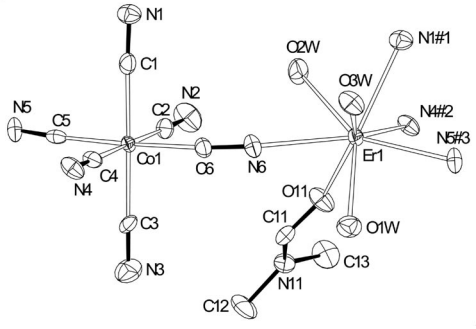

Figure 5. ORTEP drawing of **14** with 40% thermal ellipsoids; lattice water molecules and hydrogen atoms omitted for clarity (symmetry codes: #1: *–x*, 2 – *y*, *–z*; #2: *x*, *–*1 + *y*, *z*; #3: 1 + *x*, *–*1 + *y*, *z*).

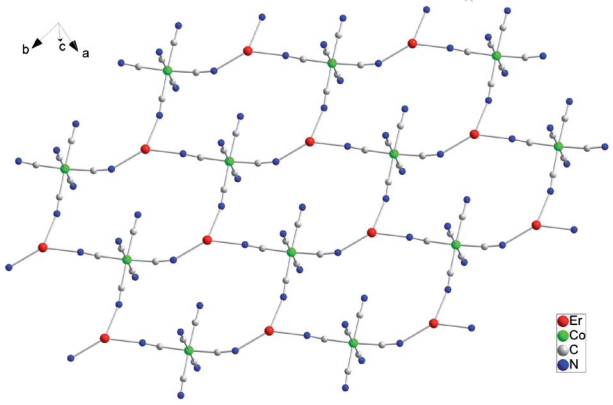

Figure 6. A sublayer of a bilayer of **14**; dmf and water molecules omitted for clarity.

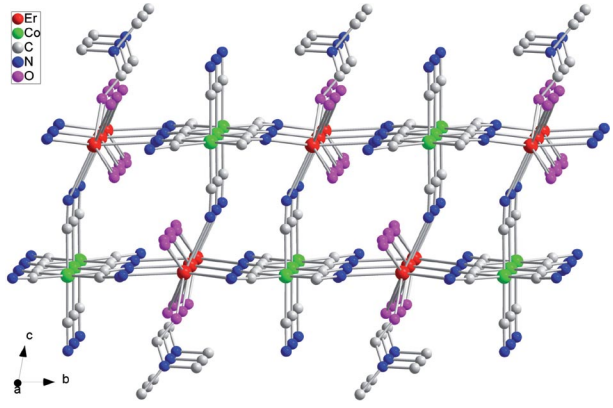

Figure 7. The bilayered structure of **14**; lattice water molecules omitted for clarity.

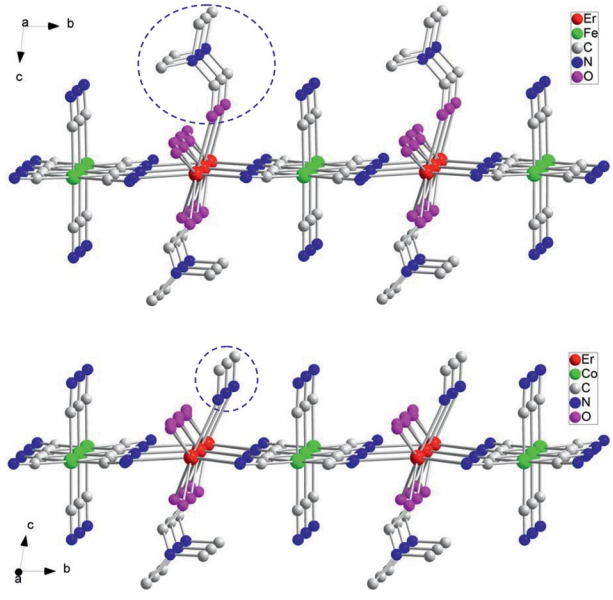

Figure 8. Top: 2D monolayer of **8**; the dmf ligand in the blue dashed circle prevents the monolayers from linking to each other further to form a bilayer. Bottom: 2D sublayer of **14**; the cyanide groups in the blue dashed circle bridge the other sublayer to form a bilayered structure.

Table 1. Nature of the reaction methods and symmetries of complexes.

LnM-dmf	Traditional solution method	Ball-milling method
Monoclinic	$Ln(H_2O)_m(dmf)_nM(CN)_6$, ($m + n = 6$,[14] 7[9b,3b,3c],5a,[15] 8,[16] M = Fe or Co)	–
Triclinic	–	$Ln(dmf)_m(H_2O)_nM(CN)_6$, ($m + n = 4$[a],[6a], 5[a],[6a], 7,[17] M = Fe or Co)
LnM-dmso	Traditional solution method	Ball-milling method
Monoclinic	$Ln(H_2O)_m(dmso)_nM(CN)_6$ ($m + n = 7$,[5b,3s,18] M = Fe or Co)	$Ln(H_2O)_m(dmso)_nM(CN)_6$ ($m + n = 3$[a], 5[a], 6[7], 7,[6b], M = Fe or Co)
Orthorhombic	$Ln(H_2O)_m(dmso)_nFe(CN)_6$ ($m + n = 7$[3s], M = Fe or Co)	$Ln(H_2O)_m(dmso)_nM(CN)_6$ ($m + n = 5$[a], M = Fe or Co)

[a] This work.

wall-, and stair-like monolayered structures, complex **14** is the second example with a bilayered structure among the 4f–3d hexacyanometalates. The first example was also reported by us,[6a] although several 3d–3d/4d/5d tetra-, hepta-, and octacyanometalates with bilayered structures have been documented by others.[12]

Generally, monolayered cyano-bridged bimetallic complexes contain three or four coplanar bridging cyanide groups, except for the stair-like structure, which contains not only three coplanar bridging cyanide groups, but also a fourth one nearly perpendicular to the plane. Unlike the stair-like monolayered structures of **1** and **2**, which contain small Ln_2M_2 "bricks", the bilayered structure of **14** comprises big Ln_3M_3 "bricks". The discrepancy probably results from the different coordination directions of the bridging cyanide groups to the lanthanide ions. The intra-sublayer Co···Er distance is 5.3622(9) Å, while the shortest intra-bilayer Co···Er separation is 7.566(1) Å. Between the adjacent bilayers, the terminal cyanide groups interact with the coordinating O1W water molecules through O–H···N hydrogen bonds, and the coordinating O2W and O3W water molecules link with the lattice O4W water molecules through O–H···O hydrogen bonds to form a 3D supramolecular hydrogen-bonding network (Figure S3). It is noteworthy that complex **14** is the first example of a hybrid prussian blue complex with a bilayered structure that contains a Co ion.[13]

Table 1 summarizes the nature of the reaction methods and symmetries of hybrid prussian blue complexes. The symmetries are monoclinic, with $P2_1/c$ (or $P2_1/a$, $P2_1/n$), without exception when the complexes with dmf as ancillary ligand were synthesized by the traditional solution method, while the symmetries are triclinic, with $P\bar{1}$, when the complexes with dmf as ancillary ligand were synthesized by the ball-milling method. However, the symmetries of complexes with dmso as ancillary ligand are monoclinic or orthorhombic regardless of the reaction methods.

Conclusions

In summary, we have demonstrated a facile and controllable approach to synthesize fourteen cyano-bridged 2D bimetallic 4f–3d assemblies with monolayered stair-like, brick-wall-like, or bilayered topologies. By controllably reducing the amount of solvent used in the reactive system, 2D monolayered stair-like and brick-wall-like structures were obtained, and then 2D bilayered topologies were prepared by further decreasing the amount of solvent. It is noteworthy that the ball-milling reaction method can be extended to Ln–$M(CN)_6$ (M = transition metal atom except for Fe and Co) systems similar to the Ln–$Fe(CN)_6$ or Ln–$Co(CN)_6$. Studies on comparing these two reaction methods and tuning the layered structures of cyano-bridged bimetallic assemblies are still in progress in our laboratory.

Experimental Section

Measurements: Elemental analyses of carbon, hydrogen, nitrogen, and sulfur were carried out with an Elementar Vario EL. Infrared spectra were obtained with a PE Spectrum-One FTIR spectrometer with KBr discs.

Syntheses: All starting materials except for $LnCl_3·6H_2O$ were commercially available and used without further purification.

$[Ln(dmso)_2(H_2O)(\mu\text{-}CN)_4Fe(CN)_2]_n$ [Ln = Gd (1) and Er (2)]: Complexes **1** and **2** were prepared by grinding the mixture of $LnCl_3·6H_2O$ (1 mmol) [Ln = Gd (**1**) and Er (**2**)], $K_3[Fe(CN)_6]$ (1 mmol, 0.329 g), and dmso (0.50 mL) in a sealed agate container for 2 h by the ball-milling method. The resulting mixture was extracted with distilled water. The filtrate was kept at room temperature for several days, and crystals suitable for X-ray analysis were obtained from the aqueous solution. Yield: 66% (based on gadolinium) for **1**. $C_{10}H_{14}FeGdN_6O_3S_2$ (543.49): calcd. C 22.09, H 2.58, N 15.47, S 11.78; found C 22.17, H 2.59, N 15.41, S 11.74. IR peaks (KBr): $\tilde{\nu}$ = 3430 (vs), 2139 (vs), 2131 (vs), 1656 (m), 1631 (s), 1421 (m), 1318 (w), 1004 (vs), 963 (s), 908 (w), 664 (w), 432(s) cm^{-1}. Yield: 74% (based on erbium) for **2**. $C_{10}H_{14}ErFeN_6O_3S_2$ (553.50): calcd. C 21.68, H 2.53, N 15.18, S 11.57; found C 21.60, H 2.52, N 15.12, S 11.61. IR peaks (KBr): $\tilde{\nu}$ = 3419 (vs), 2136 (vs), 2130 (vs), 1656 (m), 1633 (s), 1402 (m), 1320 (w), 1003 (vs), 963 (s), 905 (w), 715 (w), 429(s) cm^{-1}.

$[La(dmso)_2(H_2O)_3(\mu\text{-}CN)_3Fe(CN)_3]_n$ (3): Complex **3** was prepared by the procedure described for **1** by using $LaCl_3·6H_2O$ (1 mmol, 0.354 g) instead of $GdCl_3·6H_2O$.

$[Pr(dmso)_2(H_2O)_3(\mu\text{-}CN)_3Co(CN)_3]_n$ (4): This complex was prepared by the procedure described for **1** by using $PrCl_3·6H_2O$ (1 mmol) and $K_3[Co(CN)_6]$ (1 mmol) instead of $GdCl_3·6H_2O$ and $K_3[Fe(CN)_6]$. Yield: 75% (based on praseodymium). $C_{10}H_{18}CoN_6O_5PrS_2$ (566.26): calcd. C 21.19, H 3.18, N 14.83, S 11.30; found C 21.11, H 3.17, N 14.88, S 11.26. IR peaks (KBr): $\tilde{\nu}$ = 3351 (vs), 2136 (vs), 2126 (vs), 1659 (s), 1631 (s), 1423 (s), 1323 (m), 1000 (vs), 963 (s), 907 (w), 719 (w), 667 (s), 422(s) cm^{-1}.

$[Ln(dmf)_2(H_2O)_3(\mu\text{-}CN)_3M(CN)_3]_n \cdot nH_2O$ [Nd–Fe (5), Gd–Fe (6), Dy–Fe (7), Er–Fe (8), Nd–Co (9) and Gd–Co (10)]: Complexes **5**–**10** were prepared by the procedure described for **1** by using the corresponding $LnCl_3 \cdot 6H_2O$ (1 mmol) and dmf (0.54 mL) instead of $GdCl_3 \cdot 6H_2O$ and dmso, and $K_3[Co(CN)_6]$ instead of $K_3[Fe(CN)_6]$ in **9**–**10**. Yield: 55% (based on neodymium) for **5**. $C_{12}H_{22}FeN_8NdO_6$ (574.47): calcd. C 25.07, H 3.83, N 19.50; found C 24.98, H 3.82, N 19.43. IR peaks (KBr): $\tilde{\nu}$ = 3399 (vs), 2163 (m), 2151 (s), 2134 (vs), 1671 (s), 1650 (vs), 1496 (m), 1438 (m), 1380 (s), 1248 (m), 1116 (m), 1059 (w), 673 (s), 427(s) cm^{-1}. Yield: 62% (based on gadolinium) for **6**. $C_{12}H_{22}FeGdN_8O_6$ (587.48): calcd. C 24.51, H 3.74, N 19.06; found C 24.60, H 3.73, N 18.99. IR peaks (KBr): $\tilde{\nu}$ = 3370 (vs), 2167 (m), 2153 (s), 2135 (vs), 1654 (vs), 1497 (m), 1437 (s), 1383 (s), 1250 (m), 1116 (s), 1060 (w), 681 (m), 418(s) cm^{-1}. Yield: 68% (based on dysprosium) for **7**. $C_{12}H_{22}DyFeN_8O_6$ (592.73): calcd. C 24.29, H 3.71, N 18.90; found C 24.20, H 3.72, N 18.97. IR peaks (KBr): $\tilde{\nu}$ = 3422 (vs), 2156 (m), 2145 (s), 2126 (vs), 1656 (vs), 1495 (m), 1435 (s), 1383 (vs), 1249 (m), 1116 (m),

Table 2. Summary of crystallographic data and structure analyses for **1**–**4**.

Complexes	**1**	**2**	**3**	**4**
Formula	$C_{10}H_{14}FeGdN_6O_3S_2$	$C_{10}H_{14}ErFeN_6O_3S_2$	$C_{10}H_{18}FeLaN_6O_5S_2$	$C_{10}H_{18}CoN_6O_5PrS_2$
Fw	543.49	553.50	561.18	566.26
Color	dark yellow	brown	yellow	green
Crystal size [mm^3]	0.32 0.10 0.04	0.08 0.04 0.03	0.47 0.16 0.12	0.40 0.24 0.12
Crystal system	monoclinic	monoclinic	orthorhombic	orthorhombic
Space group	*P*2/*n*	*P*2/*n*	*Pnma*	*Pnma*
a [Å]	7.777(2)	7.748(2)	12.666(5)	12.5490(4)
b [Å]	10.673(3)	10.654(2)	14.598(6)	14.5371(4)
c [Å]	11.033(3)	10.983(3)	11.089(4)	10.9501(1)
β [°]	96.964(5)	97.19(1)	90	90
V [$Å^3$]	909.0(4)	899.5(4)	2050(1)	1997.58(9)
Z	2	2	4	4
$2\theta_{max}$ [°]	50	50	50	50
Reflections collected	2373	5794	12684	4604
Independent, observed reflections (R_{int})	1569, 1005 (0.0576)	1587, 1284 (0.0833)	1869, 1451 (0.0606)	1810, 1553 (0.0367)
$d_{calcd.}$ [g/cm^3]	1.986	2.044	1.818	1.883
μ [mm^{-1}]	4.663	5.690	2.997	3.480
T [K]	293(2)	293(2)	293(2)	293(2)
F(000)	524	532	1100	1112
*R*1, *wR*2	0.0616, 0.1087	0.0658, 0.1334	0.0376, 0.0670	0.0426, 0.1057
S	0.998	1.046	1.003	1.045
Largest and Mean Δ/σ	0, 0	0, 0	0, 0	0.001, 0
$\Delta\rho$(max/min) [$e/Å^3$]	1.376/–1.186	1.094/–1.217	1.352/–0.549	1.428/–1.335

Table 3. Summary of crystallographic data and structure analyses for **5**–**8**.

Complexes	**5**	**6**	**7**	**8**
Formula	$C_{12}H_{22}FeN_8NdO_6$	$C_{12}H_{22}FeGdN_8O_6$	$C_{12}H_{22}DyFeN_8O_6$	$C_{12}H_{22}ErFeN_8O_6$
Fw	574.47	587.48	592.73	597.49
Color	green	yellow	brown	brown
Crystal size [mm^3]	0.20 0.18 0.08	0.45 0.20 0.05	0.20 0.15 0.10	0.25 0.20 0.15
Crystal system	triclinic	triclinic	triclinic	triclinic
Space group	$P\bar{1}$	$P\bar{1}$	$P\bar{1}$	$P\bar{1}$
a [Å]	7.6984(2)	7.602(4)	7.555(4)	7.511(3)
b [Å]	9.2414(1)	9.182(5)	9.158(5)	9.128(3)
c [Å]	16.2338(3)	16.211(9)	16.177(8)	16.175(6)
α [°]	93.933(1)	94.12(6)	94.181(2)	94.237(16)
β [°]	100.286(1)	100.30(3)	100.274(5)	100.27(1)
γ [°]	101.01	101.15(4)	101.310(6)	101.31(1)
V [$Å^3$]	1109.12(4)	1086(1)	1073.1(9)	1063.2(7)
Z	2	2	2	2
$2\theta_{max}$ [°]	50	50	50	50
Reflections collected	5635	7392	6639	6576
Independent, observed reflections (R_{int})	3794, 2946 (0.0397)	3752, 3282 (0.0444)	3717, 3324 (0.0300)	3697, 3382 (0.0269)
$d_{calcd.}$ [g/cm^3]	1.720	1.797	1.834	1.866
μ [mm^{-1}]	3.010	3.738	4.174	4.645
T [K]	293(2)	293(2)	293(2)	293(2)
F(000)	568	576	580	584
*R*1, *wR*2	0.0532, 0.1283	0.0346, 0.0748	0.0326, 0.0689	0.0278, 0.0645
S	1.033	1.040	1.040	1.006
Largest and Mean Δ/σ	0.001, 0	0.001, 0	0.001, 0	0.001, 0
$\Delta\rho$(max/min) [$e/Å^3$]	2.195/–1.533	1.000/–1.025	1.469/–0.675	1.406/–0.756

1054 (m), 682(s) cm^{-1}. Yield: 77% (based on erbium) for **8**. $C_{12}H_{22}ErFeN_8O_6$ (597.49): calcd. C 24.10, H 3.68, N 18.74; found C 24.19, H 3.69, N 18.67. IR peaks (KBr): $\tilde{\nu}$ = 3431 (vs), 2158 (s), 2145 (s), 2126 (vs), 1651 (vs), 1498 (m), 1436 (s), 1382 (vs), 1249 (m), 1116 (s), 1058(w) cm^{-1}. Yield: 67% (based on neodymium) for **9**. $C_{12}H_{22}CoN_8NdO_6$ (577.55): calcd. C 24.93, H 3.81, N 19.39; found C 24.84, H 3.80, N 19.46. IR peaks (KBr): $\tilde{\nu}$ = 3400 (vs), 2164 (m), 2151 (s), 2135 (vs), 1673 (s), 1651 (vs), 1496 (m), 1437 (m), 1380 (s), 1248 (m), 1116 (s), 1059 (w), 671 (s), 428(m) cm^{-1}. Yield: 78% (based on gadolinium) for **10**. $C_{12}H_{22}CoGdN_8O_6$ (590.56): calcd. C 24.38, H 3.73, N 18.97; found C 24.29, H 3.74, N 19.04. IR peaks (KBr): $\tilde{\nu}$ = 3372 (vs), 2165 (m), 2152 (s), 2134 (s), 1654 (vs), 1498 (m), 1437 (s), 1383 (s), 1249 (m), 1115 (m), 1059 (m), 680 (s), 416(s) cm^{-1}.

$[Ln(dmso)_2(H_2O)_3(\mu\text{-}CN)_3Co(CN)_3]_n \cdot nH_2O$ [Ln = Pr (11), Nd (12) and Sm (13)]: Complexes **11**–**13** were prepared by the procedure described for **1** by using the corresponding $LnCl_3 \cdot 6H_2O$ (1 mmol) and $K_3[Co(CN)_6]$ (1 mmol) instead of $GdCl_3 \cdot 6H_2O$ and $K_3[Fe(CN)_6]$. Yield: 80% (based on praseodymium) for **11**. $C_{10}H_{20}CoN_6O_6PrS_2$ (584.28): calcd. C 20.54, H 3.42, N 14.38, S 10.95; found C 20.47, H 3.41, N 14.43, S 10.91. IR peaks (KBr): $\tilde{\nu}$ = 3379 (vs), 2159 (s), 2131 (vs), 1647 (s), 1545 (w), 1415 (s), 1318 (m), 1008 (vs), 960 (vs), 906 (w), 716 (m), 613 (m), 410(m) cm^{-1}. Yield: 71% (based on neodymium) for **12**. $C_{10}H_{20}CoN_6NdO_6S_2$ (587.61): calcd. C 20.42, H 3.40, N 14.30, S 10.89; found C 20.35, H 3.41, N 14.35, S 10.85. IR peaks (KBr): $\tilde{\nu}$ = 3417 (vs), 2148 (vs), 2138 (vs), 2127 (s), 1664 (s), 1497 (m), 1437 (m), 1381 (s), 1252 (w), 1118 (m), 1007 (vs), 961 (m), 684 (m), 432(m) cm^{-1}. Yield: 81% (based on samarium) for **13**. $C_{10}H_{20}CoN_6O_6S_2Sm$ (593.72): calcd. C 20.21, H 3.37, N 14.14, S 10.78; found C 20.13, H 3.38, N 14.19, S 10.79. IR peaks (KBr): $\tilde{\nu}$ = 3533 (vs), 3366 (vs), 2151 (vs), 2140 (vs), 2130 (s), 1657 (m), 1622 (m), 1438 (w), 1415 (w), 1401 (w), 1321 (w), 1110 (vs), 962 (s), 906 (w), 717 (w), 616 (m), 431(s) cm^{-1}.

$[Er(dmf)(H_2O)_3(\mu\text{-}CN)_4Co(CN)_2]_n \cdot nH_2O$ (14): This complex was prepared by the procedure described for **1** by using $ErCl_3 \cdot 6H_2O$ (1 mmol, 0.382 g), $K_3[Co(CN)_6]$ (1 mmol, 332 mg), and dmf (0.27 mL). Yield: 60% (based on erbium). $C_9H_{15}CoErN_7O_5$ (527.47): calcd. C 20.48, H 2.84, N 18.58; found C 20.41, H 2.83, N 18.65. IR peaks (KBr): $\tilde{\nu}$ = 3428 (vs), 2168 (vs), 2157 (vs), 2139 (vs), 1669 (vs), 1497 (m), 1436 (s), 1376 (s), 1249 (m), 1122 (s), 1057(w) cm^{-1}.

Table 5. Summary of crystallographic data and structure analyses for **13** and **14**.

Complexes	**13**	**14**
Formula	$C_{10}H_{20}CoN_6O_6S_2Sm$	$C_9H_{15}CoErN_7O_5$
Fw	593.72	527.47
Color	light yellow	colorless
Crystal size [mm^3]	0.30 0.12 0.03	0.09 0.04 0.03
Crystal system	monoclinic	triclinic
Space group	$P2_1/c$	$P\bar{1}$
a [Å]	7.635(4)	7.4334(5)
b [Å]	30.776(1)	8.9994(4)
c [Å]	9.114(4)	12.905(1)
α [°]	90	78.86(2)
β [°]	100.621(5)	85.13(2)
γ [°]	90	79.06(1)
V [$Å^3$]	2104.9(1)	830.6(1)
Z	4	2
$2\theta_{max}$ [°]	50	50
Reflections collected	12778	5558
Independent, observed reflections (R_{int})	3674, 3147 (0.0482)	2922, 2502 (0.0475)
$d_{calcd.}$ [g/cm^3]	1.873	2.109
μ [mm^{-1}]	3.784	6.050
T [K]	293(2)	293(2)
F(000)	1164	506
*R*1, *wR*2	0.0427, 0.1018	0.0467, 0.1041
S	1.036	1.018
Largest and Mean Δ/σ	0.003, 0	0.001, 0
$\Delta\rho$(max/min) [$e/Å^3$]	1.787/–0.840	1.827/–1.092

Table 4. Summary of crystallographic data and structure analyses for **9**–**12**.

Complexes	**9**	**10**	**11**	**12**
Formula	$C_{12}H_{22}CoN_8NdO_6$	$C_{12}H_{22}CoGdN_8O_6$	$C_{10}H_{20}CoN_6O_6PrS_2$	$C_{10}H_{20}CoN_6NdO_6S_2$
Fw	577.55	590.56	584.28	587.61
Color	blue	colorless	light green	purple
Crystal size [mm^3]	0.34 0.22 0.18	0.15 0.10 0.05	0.49 0.42 0.30	0.18 0.10 0.02
Crystal system	triclinic	triclinic	monoclinic	monoclinic
Space group	$P\bar{1}$	$P\bar{1}$	$P2_1/c$	$P2_1/c$
a [Å]	7.6631(5)	7.564(3)	7.706(3)	7.6800(6)
b [Å]	9.1685(6)	9.105(3)	30.834(1)	30.930(2)
c [Å]	16.209(1)	16.165(6)	9.149(3)	9.1225(7)
α [°]	93.92	94.072(2)	90	90
β [°]	100.38	100.308(6)	100.629(3)	100.661(2)
γ [°]	101.111(1)	101.243(4)	90	90
V [$Å^3$]	1092.9(1)	1067.8(7)	2136.5(1)	2129.6(3)
Z	2	2	4	4
$2\theta_{max}$ [°]	50	50	50	50
Reflections collected	5682	6620	13270	7228
Independent, observed reflections (R_{int})	3804, 3460 (0.0236)	3713, 3338 (0.0265)	3757, 3515 (0.0487)	3729, 2284 (0.0715)
$d_{calcd.}$ [g/cm^3]	1.755	1.837	1.816	1.833
μ [mm^{-1}]	3.150	3.898	3.260	3.421
T [K]	293(2)	293(2)	293(2)	293(2)
F(000)	570	578	1152	1156
*R*1, *wR*2	0.0379, 0.0909	0.0300, 0.0621	0.0471, 0.1153	0.0689, 0.1128
S	1.054	1.064	1.054	1.045
Largest and Mean Δ/σ	0.001, 0	0.001, 0	0.004, 0	0.003, 0
$\Delta\rho$(max/min) [$e/Å^3$]	0.915/–0.981	1.007/–0.615	1.202/–0.931	0.741/–1.321

X-ray Crystallographic Studies: The intensity data sets were collected with Rigaku Mercury CCD (**2**, **3**, **6**, **7**, **8**, **10**, **11**, **13**, and **14**) and Siemens SMART CCD (**1**, **4**, **5**, **9**, and **12**) X-ray diffractometers with graphite monochromated Mo-K_α radiation (λ = 0.71073 Å) by using a ω scan technique. CrystalClear (**2**, **3**, **6**, **7**, **8**, **10**, **11**, **13**, and **14**) and Siemens SAINT (**1**, **4**, **5**, **9**, and **12**) software was used for data reduction and empirical absorption corrections.[19] The structures were solved by direct methods with the Siemens SHELXTL™ Version 5 package of crystallographic software.[20] The difference Fourier maps based on these atomic positions yield the other non-hydrogen atoms. The hydrogen atom positions were generated symmetrically, allowed to ride on their respective parent atoms, and included in the structure factor calculations with assigned isotropic thermal parameters, but they were not refined. Additionally, the hydrogen atoms on disordered dmso ligands were not generated because of the disorder of the sulfur atoms. The structures were refined by using a full-matrix least-squares refine-

Table 6. Selected bond lengths [Å] and bond angles [°] of **1** and **2**.

	1 [Gd–Fe]$_n$	**2** [Er–Fe]$_n$
Ln1–O11 ×2	2.324(3)	2.322(3)
Ln1–O1W	2.336(5)	2.295(5)
Ln1–N1#1 ×2	2.466(4)	2.450(4)
Ln1–N3 ×2	2.510(4)	2.511(4)
M1–C1 ×2	1.954(4)	1.955(5)
M1–C2 ×2	1.949(4)	1.938(5)
M1–C3 ×2	1.969(4)	1.945(5)
C1–N1	1.131(6)	1.123(6)
C2–N2	1.126(6)	1.133(6)
C3–N3	1.140(5)	1.137(6)
N1–C1–M1	176.9(4)	175.0(4)
N2–C2–M1	174.7(4)	177.7(4)
N3–C3–M1	176.9(4)	177.5(4)
C1–N1–M1#1	170.8(3)	170.2(4)
C3–N3–M1	169.0(3)	169.9(4)

Symmetry codes: #1 $-x + 1, -y + 1, -z + 1$.

Table 7. Selected bond lengths [Å] and bond angles [°] of **3** and **4**.

	3 [La–Fe]$_n$	**4** [Pr–Co]$_n$
Ln1–O11 ×2	2.401(3)	2.367(3)
Ln1–O1W	2.727(4)	2.701(5)
Ln1–O2W ×2	2.523(3)	2.481(3)
Ln1–N1#1	2.614(5)	2.568(5)
Ln1–N2#2	2.619(5)	2.576(6)
Ln1–N5	2.630(5)	2.587(6)
M1–C1	1.917(6)	1.875(6)
M1–C2	1.926(6)	1.885(6)
M1–C3 ×2	1.927(4)	1.903(5)
M1–C4	1.937(5)	1.891(6)
M1–C5	1.946(6)	1.900(6)
C1–N1	1.138(7)	1.149(8)
C2–N2	1.156(7)	1.168(8)
C3–N3	1.159(5)	1.139(6)
C4–N4	1.136(6)	1.150(8)
C5–N5	1.140(7)	1.160(8)
N1–C1–M1	178.2(5)	177.4(6)
N2–C2–M1	172.3(5)	171.6(5)
N3–C3–M1	178.5(4)	178.3(4)
N4–C4–M1	173.9(5)	175.6(6)
N5–C5–M1	175.2(5)	172.5(6)
C1–N1–Ln1#3	158.0(4)	159.7(5)
C2–N2–Ln1#4	160.2(4)	161.2(5)
C5–N5–Ln1	178.8(5)	179.6(5)

Symmetry codes: #1 $x, y, z + 1$; #2 $x - 1/2, y, -z - 1/2$; #3 $x, y, z - 1$; #4 $x + 1/2, y, -z - 1/2$.

Table 8. Selected bond lengths [Å] and bond angles [°] of **5**–**10**.

	5 [Nd–Fe]$_n$	**6** [Gd–Fe]$_n$	**7** [Dy–Fe]$_n$	**8** [Er–Fe]$_n$	**9** [Nd–Co]$_n$	**10** [Gd–Co]$_n$
Ln1–O11	2.399(3)	2.341(2)	2.318(2)	2.290(2)	2.394(3)	2.318(3)
Ln1–O21	2.368(3)	2.322(3)	2.289(2)	2.269(2)	2.358(3)	2.338(3)
Ln1–O1W	2.503(3)	2.437(3)	2.407(2)	2.380(2)	2.493(3)	2.442(3)
Ln1–O2W	2.497(3)	2.439(2)	2.406(2)	2.389(2)	2.491(3)	2.436(3)
Ln1–O3W	2.480(3)	2.433(3)	2.403(2)	2.374(2)	2.478(3)	2.425(3)
Ln1–N3#1	2.537(3)	2.488(3)	2.445(3)	2.423(2)	2.554(4)	2.497(4)
Ln1–N4#2	2.540(3)	2.495(3)	2.465(3)	2.441(2)	2.569(4)	2.495(4)
Ln1–N6	2.555(3)	2.495(3)	2.471(3)	2.442(2)	2.545(3)	2.484(4)
M1–C1	1.943(4)	1.939(3)	1.933(3)	1.937(3)	1.902(4)	1.907(5)
M1–C2	1.954(4)	1.953(3)	1.941(3)	1.941(3)	1.910(5)	1.899(5)
M1–C3	1.942(4)	1.950(3)	1.951(3)	1.943(3)	1.915(5)	1.899(5)
M1–C4	1.934(3)	1.935(3)	1.936(3)	1.937(2)	1.896(4)	1.900(5)
M1–C5	1.943(4)	1.947(3)	1.948(3)	1.940(3)	1.894(5)	1.892(5)
M1–C6	1.943(4)	1.949(3)	1.956(3)	1.950(3)	1.918(4)	1.899(5)
C1–N1	1.149(5)	1.144(4)	1.149(4)	1.146(4)	1.149(6)	1.152(6)
C2–N2	1.138(6)	1.133(4)	1.149(4)	1.146(4)	1.144(6)	1.148(6)
C3–N3	1.158(5)	1.136(4)	1.146(4)	1.149(3)	1.127(6)	1.138(6)
C4–N4	1.155(4)	1.151(4)	1.148(4)	1.141(3)	1.149(5)	1.142(6)
C5–N5	1.144(5)	1.135(4)	1.143(4)	1.138(4)	1.152(6)	1.150(6)
C6–N6	1.156(5)	1.154(4)	1.144(4)	1.148(4)	1.131(5)	1.149(6)
N1–C1–M1	179.0(4)	177.4(3)	178.2(3)	178.2(3)	175.2(4)	178.5(4)
N2–C2–M1	177.5(4)	177.2(3)	177.9(3)	177.8(3)	176.6(5)	174.2(5)
N3–C3–M1	177.3(3)	176.6(3)	176.4(3)	177.5(2)	179.1(5)	178.8(4)
N4–C4–M1	170.8(3)	173.6(3)	171.9(3)	170.4(2)	173.6(4)	176.8(5)
N5–C5–M1	174.9(3)	174.3(3)	174.3(3)	174.2(2)	177.7(4)	172.0(4)
N6–C6–M1	177.8(3)	178.9(3)	179.3(3)	179.7(2)	176.8(4)	177.1(4)
C3–N3–Ln1#3	175.3(3)	175.6(3)	174.7(3)	175.9(2)	150.3(3)	165.7(4)
C4–N4–Ln1#4	153.0(3)	151.2(3)	152.9(3)	154.9(2)	165.2(3)	152.2(4)
C6–N6–Ln1	165.5(3)	165.7(2)	166.8(2)	166.9(2)	175.6(4)	174.8(4)

Symmetry codes: #1 $x + 1, y, z$; #2 $x, y - 1, z$; #3 $x - 1, y, z$; #4 $x, y + 1, z$.

ment on F^2. All atoms except for hydrogen atoms were refined anisotropically.

CCDC-282487 (for **1**), -282481 (for **2**), -750231 (for **3**), -282488 (for **4**), -268690 (for **5**), -268692 (for **6**), -750230 (for **7**), -282491 (for **8**), -268691 (for **9**), -268693 (for **10**), -282482 (for **11**), -282483 (for **12**), -282484 (for **13**), and -282490 (for **14**) contain the supplementary crystallographic data for this paper. These data can be obtained free of charge from The Cambridge Crystallographic Data Centre via www.ccdc.cam.ac.uk/data_request/cif.

Crystal Structures: The summary of crystallographic data and structure analyses for **1**–**14** are listed in Tables 2, 3, 4, and 5.

Table 9. Selected bond lengths [Å] and bond angles [°] of **11**–**13**.

	11 [Pr–Co]$_n$	**12** [Nd–Co]$_n$	**13** [Sm-Co]$_n$
Ln1–O11	2.361(2)	2.403(3)	2.382(2)
Ln1–O21	2.418(3)	2.348(3)	2.331(2)
Ln1–O1W	2.498(3)	2.477(3)	2.443(2)
Ln1–O2W	2.481(2)	2.458(3)	2.442(2)
Ln1–O3W	2.496(2)	2.496(3)	2.458(2)
Ln1–N3#1	2.598(3)	2.576(4)	2.553(2)
Ln1–N5#2	2.591(3)	2.562(4)	2.550(2)
Ln1–N6	2.574(3)	2.543(3)	2.518(2)
M1–C1	1.893(3)	1.893(5)	1.904(2)
M1–C2	1.906(3)	1.922(5)	1.885(3)
M1–C3	1.903(3)	1.894(4)	1.898(2)
M1–C4	1.898(3)	1.885(4)	1.899(2)
M1–C5	1.895(3)	1.889(4)	1.898(2)
M1–C6	1.893(3)	1.904(4)	1.903(2)
C1–N1	1.146(4)	1.118(6)	1.147(3)
C2–N2	1.142(4)	1.125(6)	1.143(3)
C3–N3	1.139(4)	1.143(6)	1.136(3)
C4–N4	1.135(5)	1.154(5)	1.145(3)
C5–N5	1.130(4)	1.154(5)	1.136(3)
C6–N6	1.145(4)	1.145(5)	1.146(3)
N1–C1–M1	178.2(3)	177.1(4)	177.1(2)
N2–C2–M1	177.0(3)	178.9(4)	179.1(2)
N3–C3–M1	178.5(3)	174.6(4)	175.2(2)
N4–C4–M1	173.6(3)	178.4(4)	178.5(2)
N5–C5–M1	172.8(3)	172.6(4)	173.7(2)
N6–C6–M1	176.6(3)	176.4(4)	175.7(2)
C3–N3–Ln1#3	162.1(3)	162.4(3)	161.5(2)
C5–N5–Ln1#4	153.1(3)	152.7(3)	153.4(2)
C6–N6–Ln1	169.3(3)	171.4(4)	171.6(2)

Symmetry codes: #1 $x + 1, y, z$; #2 $x + 1, y, z + 1$; #3 $x - 1, y, z$; #4 $x - 1, y, z - 1$.

Table 10. Selected bond lengths [Å] and bond angles [°] of **14**.

Er1–O11	2.251(3)	C2–N2	1.138(8)
Er1–O1W	2.384(4)	C3–N3	1.134(7)
Er1–O2W	2.377(4)	C4–N4	1.129(7)
Er1–O3W	2.352(4)	C5–N5	1.156(6)
Er1–N1#1	2.457(4)	C6–N6	1.168(6)
Er1–N4#2	2.440(5)	N1–C1–Co1	176.9(5)
Er1–N5#3	2.406(4)	N2–C2–Co1	176.3(5)
Er1–N6	2.480(4)	N3–C3–Co1	177.6(5)
Co1–C1	1.885(5)	N4–C4–Co1	176.9(5)
Co1–C2	1.896(6)	N5–C5–Co1	175.7(5)
Co1–C3	1.900(5)	N6–C6–Co1	171.8(5)
Co1–C4	1.913(6)	C1–N1–Er1#1	157.2(4)
Co1–C5	1.895(5)	C4–N4–Er1#4	166.4(4)
Co1–C6	1.870(5)	C5–N5–Er1#5	170.4(4)
C1–N1	1.147(6)	C6–N6–Er1	151.4(4)

Symmetry codes: #1 $-x, -y + 2, -z$; #2 $x, y - 1, z$; #3 $x + 1, y - 1, z$; #4 $x, y + 1, z$; #5 $x - 1, y + 1, z$.

Selected bond lengths and bond angles are given in Tables 6, 7, 8, 9, and 10.

Supporting Information (see footnote on the first page of this article): Packing diagrams for complexes **1**, **8**, and **14**.

Acknowledgments

We gratefully acknowledge financial support by the National Natural Science Foundation (NSF) of China (20701037, 90922035), 973 program (2009CB939801), Key Project from the CAS (KJCX2.YW.M10, KJCX2.YW.319), and the National Natural Science Foundation (NSF) of Fujian Province (2008I0026).

[1] a) D. Papanikolaou, S. Margadonna, W. Kosaka, S. Ohkoshi, M. Brunelli, K. Prassides, *J. Am. Chem. Soc.* **2006**, *128*, 8358–8363; b) K. W. Chapman, P. J. Chupas, C. J. Kepert, *J. Am. Chem. Soc.* **2006**, *128*, 7009–7014; c) S. Ohkoshi, H. Tokoro, T. Hozumi, Y. Zhang, K. Hashimoto, C. Mathonière, I. Bord, G. Rombaut, M. Verelst, C. C. Moulin, F. Villain, *J. Am. Chem. Soc.* **2006**, *128*, 270–277; d) C.-F. Wang, J.-L. Zuo, B. M. Bartlett, Y. Song, J. R. Long, X.-Z. You, *J. Am. Chem. Soc.* **2006**, *128*, 7162–7163; e) S. Ohkoshi, Y. Hamada, T. Matsuda, Y. Tsunobuchi, H. Tokoro, *Chem. Mater.* **2008**, *20*, 3048–3054; f) H. Zhou, Y. Y. Chen, A. H. Yuan, X. P. Shen, *Inorg. Chem. Commun.* **2008**, *11*, 363–366; g) S. L. Ma, Y. Ma, S. Ren, S. P. Yan, P. Cheng, Q. L. Wang, D. Z. Liao, *Cryst. Growth Des.* **2008**, *8*, 3761–3765; h) Y. Jin, Y. Qi, S. R. Batten, P. Cao, W. Chen, Y. Che, J. Zheng, *Inorg. Chim. Acta* **2009**, *362*, 3395–3400.

[2] a) F. Hulliger, M. Landolt, H. Vetsch, *J. Solid State Chem.* **1976**, *18*, 283–291; b) V. Gadet, T. Mallah, I. Castro, M. Verdaguer, *J. Am. Chem. Soc.* **1992**, *114*, 9213–9214; c) Ø. Hatlevik, W. E. Buschmann, J. Zhang, J. L. Manson, J. S. Miller, *Adv. Mater.* **1999**, *11*, 914–918; d) S. Margadonna, K. Prassides, A. N. Fitch, *Angew. Chem. Int. Ed.* **2004**, *43*, 6316–6319.

[3] a) J. G. Moore, E. J. Lochner, C. Ramsey, N. S. Dalal, A. E. Stiegman, *Angew. Chem. Int. Ed.* **2003**, *42*, 2741–2743; b) A. Figuerola, C. Diaz, J. Ribas, V. Tangoulis, J. Granell, F. Lloret, J. Mahia, M. Maestro, *Inorg. Chem.* **2003**, *42*, 641–649; c) J.-R. Li, L.-Z. Cai, G.-C. Guo, X.-H. Bu, J.-S. Huang, *Acta Crystallogr., Sect. E* **2004**, *60*, m259–m261; d) H. Tokoro, S. Ohkoshi, T. Matsuda, K. Hashimoto, *Inorg. Chem.* **2004**, *43*, 5231–5236; e) M. K. Saha, F. Lloret, I. Bernal, *Inorg. Chem.* **2004**, *43*, 1969–1975; f) C. P. Berlinguette, A. Dragulescu-Andrasi, A. Sieber, J. R. Galan-Mascaros, H.-U. Gudel, C. Achim, K. R. Dunbar, *J. Am. Chem. Soc.* **2004**, *126*, 6222–6223; g) F. H. Kohler, R. Lescouezec, *Angew. Chem. Int. Ed.* **2004**, *43*, 2571–2573; h) G. M. Li, O. Sato, T. Akitsu, Y. Einaga, *J. Solid State Chem.* **2004**, *177*, 3835–3838; i) S.-H. Liang, Y.-X. Che, J.-M. Zheng, *Jiegou Huaxue (Chin.) (Chin. J. Struct. Chem.)* **2005**, *24*, 7–12; j) T. Hozumi, K. Hashimoto, S. Ohkoshi, *J. Am. Chem. Soc.* **2005**, *127*, 3864–3869; k) S. Ikeda, T. Hozumi, K. Hashimoto, S. Ohkoshi, *Dalton Trans.* **2005**, 2120–2123; l) M. K. Saha, M. C. Morón, F. Palacio, I. Bernal, *Inorg. Chem.* **2005**, *44*, 1354–1361; m) F. Bonadio, M. C. Senna, J. Ensling, A. Sieber, A. Neels, H. Stoeckli-Evans, S. Decurtins, *Inorg. Chem.* **2005**, *44*, 969–978; n) I. P. Y. Shek, W.-F. Yeung, T.-C. Lau, J. Zhang, S. Gao, L. Szeto, W.-T. Wong, *Eur. J. Inorg. Chem.* **2005**, 364–370; o) S. B. Artemkina, N. G. Naumov, A. V. Virovets, V. E. Fedorov, *Eur. J. Inorg. Chem.* **2005**, 142–146; p) J. R. Withers, C. Ruschmann, P. Bojang, S. Parkin, S. M. Holmes, *Inorg. Chem.* **2005**, *44*, 352–358; q) H. Zhao, N. L. A. Prosvirin, H. T. Chifotides, K. R. Dunbar, *Dalton Trans.* **2007**, 878–888; r) X. Zhu, W. K. Wong, J. Guo, W. Y. Wong, J. P. Zhang, *Eur. J. Inorg. Chem.* **2008**, 3515–3523; s) J.-R. Li, W.-T. Chen, M.-L. Tong, G.-C. Guo, Y. Tao, Q. Yu, W.-C. Song, X.-H. Bu, *Cryst. Growth Des.* **2008**, *8*, 2780–2792; t) Y.-F. Huang, H.-H. Wei, M. Katada, *J. Coord. Chem.* **2008**, *61*, 2683–2689.

[4] a) K. Halbauer, H. Gorls, T. Fidler, W. Imhof, *J. Organomet. Chem.* **2007**, *692*, 1898–1911; b) N. Yanai, W. Kaneko, K. Yoneda, M. Ohba, S. Kitagawa, *J. Am. Chem. Soc.* **2007**, *129*, 3496–3497; c) W. Kaneko, S. Kitagawa, M. Ohba, *J. Am. Chem. Soc.* **2007**, *129*, 248–249; d) J. Zhang, A. Lachgar, *J. Am. Chem. Soc.* **2007**, *129*, 250–251; e) M. G. Hilfiger, M. Shatruk, A. Prosvirin, K. R. Dunbar, *Chem. Commun.* **2008**, 5752–5754; f) M. Atanasov, C. Busche, P. Comba, F. ElHallak, B. Martin, G. Rajaraman, J. van Slageren, H. Wadepohl, *Inorg. Chem.* **2008**, *47*, 8112–8125; g) O. Sereda, A. Neels, F. Stoeckli, H. Stoeckli-Evans, Y. Filinchuk, *Cryst. Growth Des.* **2008**, *8*, 2307–2311; h) Y. Yoshida, K. Inoue, M. Kurmoo, *Chem. Lett.* **2008**, *37*, 504–505; i) K. Halbauer, H. Gorls, T. Fidler, W. Imhof, *Z. Anorg. Allg. Chem.* **2008**, *634*, 1921–1928; j) O. Sereda, J. Ribas, H. Stoeckli-Evans, *Inorg. Chem.* **2008**, *47*, 5107–5113.

[5] a) J. R. Li, L.-Z. Cai, Y. Zheng, G.-C. Guo, X. H. Bu, J.-S. Huang, *Chin. J. Inorg. Chem.* **2003**, *19*, 91–94; b) W.-T. Chen, L.-Z. Cai, A.-Q. Wu, G.-C. Guo, J.-S. Huang, *Chin. J. Struct. Chem.* **2004**, *23*, 1282–1286.

[6] a) W.-T. Chen, M.-S. Wang, L.-Z. Cai, G. Xu, T. Akitsu, M. A. Tanaka, G.-C. Guo, J.-S. Huang, *Cryst. Growth Des.* **2006**, *6*, 1738–1741; b) W.-T. Chen, G.-C. Guo, M.-S. Wang, G. Xu, L.-Z. Cai, T. Akitsu, M. Akita-Tanaka, A. Matsushita, J.-S. Huang, *Inorg. Chem.* **2007**, *46*, 2105–2114.

[7] W.-T. Chen, G.-C. Guo, L.-Z. Cai, H.-F. Chen, G. Xu, J.-S. Huang, *Chin. J. Struct. Chem.* **2007**, *26*, 1239–1242.

[8] a) H.-Z. Kou, W.-M. Bu, S. Gao, D.-Z. Liao, Z.-H. Jiang, S.-P. Yan, Y.-G. Fan, G.-L. Wang, *J. Chem. Soc., Dalton Trans.* **2000**, 2996–3000; b) H. Miyasaka, H. Ieda, N. Matsumoto, K. Sugiura, M. Yamashita, *Inorg. Chem.* **2003**, *42*, 3509–3515.

[9] a) B. Yan, Z. Chen, *Chem. Lett.* **2000**, 1244–1245; b) B. Yan, Z. Chen, *Helv. Chim. Acta* **2001**, *84*, 817–829.

[10] a) A. Dommann, H. Vetsch, F. Hulliger, W. Petter, *Acta Crystallogr., Sect. C* **1990**, *46*, 1992–1994; b) D. F. Mullica, J. M. Farmer, B. P. Cunningham, J. A. Kautz, *J. Coord. Chem.* **2000**, *49*, 239–250.

[11] C. Yang, G.-C. Guo, H.-W. Ma, J.-C. Liu, X. Zhang, F.-K. Zheng, S.-H. Lin, G.-W. Zhou, J.-G. Mao, J.-S. Huang, *Chin. J. Struct. Chem.* **2001**, *20*, 229–232.

[12] a) I. Muga, J. M. Gutiérrez-Zorrilla, P. Vitoria, P. Román, L. Lezama, J. I. Beitia, *Eur. J. Inorg. Chem.* **2004**, 1886–1893; b) X. F. Le Goff, S. Willemin, C. Coulon, J. Larionova, B. Donnadieu, R. Clérac, *Inorg. Chem.* **2004**, *43*, 4784–4786; c) R. Kania, K. Lewiński, B. Sieklucka, *Dalton Trans.* **2003**, 1033–1040.

[13] A. Figuerola, J. Ribas, D. Casanova, M. Maestro, S. Alvarez, C. Diaz, *Inorg. Chem.* **2005**, *44*, 6949–6958.

[14] C. H. Ge, H. Z. Kou, Z. H. Ni, Y. B. Jiang, L. F. Zhang, A. L. Cui, O. Sato, *Chem. Lett.* **2005**, *34*,1280–1281.

[15] a) J. R. Li, G.-C. Guo, M.-S. Wang, G.-W. Zhou, X. H. Bu, J.-S. Huang, *Chin. J. Struct. Chem.* **2003**, *22*, 182–186; b) G. M. Li, T. Akitsu, O. Sato, Y. Einaga, *J. Am. Chem. Soc.* **2003**, *125*, 12396–12397; c) G. M. Li, T. Akitsu, O. Sato, Y. Einaga, *J. Coord. Chem.* **2004**, *57*, 855–864; d) J. R. Li, L.-Z. Cai, R. Q. Zou, G.-W. Zhou, G.-C. Guo, X. H. Bu, J.-S. Huang, *Acta Crystallogr., Sect. E* **2002**, *58*, m686–m687; e) J. A. Kautz, D. F. Mullica, B. P. Cunningham, R. A. Combs, J. M. Farmer, *J. Mol. Struct.* **2000**, *523*, 175–182; f) G. M. Li, T. Akitsu, O. Sato, Y. Einaga, *J. Coord. Chem.* **2004**, *57*, 189–198; g) T. Akitsu, Y. Einaga, *Polyhedron* **2006**, *25*, 2655–2662; h) B. P. Cunningham, J. A. Kautz, *J. Chem. Crystallogr.* **2000**, *30*, 671–675; i) T. Akitsu, Y. Einaga, *Chem. Papers* **2007**, *61*, 194–198.

[16] a) Y. Dai, X. Y. Chen, P. Cheng, D. Z. Liao, S. P. Yan, Z. H. Jiang, *Trans. Met. Chem.* **2004**, *29*, 12–15; b) H. Z. Kou, G. M. Yang, D. Z. Liao, P. Cheng, Z. H. Jiang, S. P. Yan, X. Y. Huang, G. L. Wang, *J. Chem. Crystallogr.* **1998**, *28*, 303–307.

[17] W.-T. Chen, L.-Z. Cai, A.-Q. Wu, G.-C. Guo, J.-S. Huang, *Chin. J. Inorg. Chem.* **2004**, *20*, 693–697.

[18] Z.-Q. Zhao, W.-T. Chen, X. Liu, L.-Z. Cai, G.-C. Guo, J.-S. Huang, *Chin. J. Struct. Chem.* **2006**, *25*, 1481–1486.

[19] Rigaku (**2002**), *CrystalClear Version 1.35*, Rigaku Corporation; Siemens (**1994**), SAINT Software Reference Manual, Siemens Energy & Automation Inc., Madison, Wisconsin, USA.

[20] Siemens (**1994**), *SHELXTL*^{TM} Version 5 Reference Manual, Siemens Energy & Automation Inc., Madison, Wisconsin, USA.

Received: February 1, 2010
Published Online: May 25, 2010

